Available online at www.sciencedirect.com

jmr&t Journal of Materials Research and Technology

https://www.journals.elsevier.com/journal-of-materials-research-and-technology

Original Article

The effect of cesium dopant on APCVD graphene coating on copper

Samira Naghdi[a], Katarina Nešović[b], Gonzalo Sánchez-Arriaga[a], Hyun Yong Song[c,d], Sung Wng Kim[c,d], Kyong Yop Rhee[e,*], Vesna Mišković-Stanković[b,e,*]

[a] Bioengineering and Aerospace Engineering Department, Universidad Carlos III de Madrid, 28911 Leganés, Spain
[b] Faculty of Technology and Metallurgy, University of Belgrade, Karnegijeva 4, 11000 Belgrade, Serbia
[c] Energy Science Department, Sungkyunkwan University, Suwon, Republic of Korea
[d] Center for Integrated Nanostructure Physics (CINAP), Institute for Basic Science (IBS), Sungkyunkwan University, Suwon, Republic of Korea
[e] Department of Mechanical Engineering, Kyung Hee University, 17104 Yongin, Republic of Korea

ARTICLE INFO

Article history:
Received 15 April 2020
Accepted 29 June 2020
Available online 16 July 2020

Keywords:
Graphene
Doping
XPS
Raman spectroscopy
EIS
Polarization

ABSTRACT

This study reports *in-situ* cesium-doped graphene (G/Cs) coating obtained by introducing Cs_2CO_3 into the atmospheric pressure chemical vapor deposition (APCVD) furnace during graphene deposition on copper. The successful Cs-doping of the graphene coating was confirmed via X-ray photoelectron spectroscopy (XPS). As compared to the spectra of pure graphene coating, the XPS spectra of the G/Cs coating revealed a shift of the C1s and $Cs3d_{5/2}$ peaks to higher and lower binding energies, respectively; thus, implying the n-type character of the doping and indicating a charge transfer between Cs and graphene. Raman results show that a pure graphene coating is composed of fewer layers, fewer defects, and larger domain size than the G/Cs coating. Ultraviolet photoelectron spectroscopy was utilized to study the work function of graphene and the G/Cs and revealed that doping graphene with Cs dopants reduced the work function of graphene by 1.2 eV. Electrochemical testing during 15-day immersion in 0.1 M NaCl indicated the destructive effect of the G/Cs coating on the Cu substrate. The results showed that the G/Cs coating exhibits a higher corrosion rate and lower corrosion resistance than even the bare metal itself.

1. Introduction

Due to its extraordinary properties, a significant research effort on the development of graphene coatings has been carried out in the last two decades. Several methods to control the characteristics of graphene, including chemical and physical approaches, have been reported [1]. The thermal annealing [2,3], chemical functionalization [4,5], changing the number of graphene layers [6], engineering the defects and disorders of the graphene layers [7], irradiation of graphene via different types of radiation [8,9] (i.e., plasma, UV, IR, etc.) are all different approaches to modify specific characteristics of graphene. Among all these characteristics, changing the Fermi level and

* Corresponding authors.
E-mails: rheeky@khu.ac.kr (K.Y. Rhee), vesna@tmf.bg.ac.rs (V. Mišković-Stanković).
https://doi.org/10.1016/j.jmrt.2020.06.091

the work function of the graphene is one of the most interesting. Graphene is a zero bandgap semiconductor, and the control of the Fermi level opens a wide range of electrical, thermionic, and optical applications [10].

Due to the serious dilemmas, regarding the usage of the conventional conductive transparent metal oxides (such as ITO) [11], graphene shows potential as an alternative for conventional conductive transparent metal oxides, and replacing them with graphene would have a revolutionary impact on the size, cost, weight, and functions of future electronic and optoelectronic devices. The impressive ability of graphene to serve as both cathode and anode in electronic and optoelectronic devices is undeniable due to the tunable work function of graphene [10]. Application of graphene as cathode demands lowering its work function that can be achieved by n-doping, and in this regard alkali metals have been reported as some of the most effective dopants [12].

Kwon et al. used wet chemical doping to lower the work function of graphene [12]. They used alkali metal carbonate as the precursor of n-dopant agents. In three steps, they synthesized graphene and doped graphene with the alkali metal solution. They could lower the work function of graphene from 4.25 eV to 3.4 eV, but due to the formation of metal particles on the graphene layer, the optical transmittance of the graphene layer was diminished. Chang et al. reported a multi-step process to produce, transfer, and dope the graphene layers with alkali metals for application as a top cathode in blue organic light-emitting diodes [13]. Using their n-doping procedure, they could reduce the graphene's work function from 4.2 eV to 3.2 eV. Since this doping procedure was a multi-step process, it was time-consuming, and altering the final product quality was inevitable. Park et al. investigated the tunability of the graphene's charge transport and work function by wet chemical doping of alkali metal carbonates for application in n-channel thin-film transistors (TFTs) [14]. Although alkali metal carbonates improved the carrier injection in n-channel TFTs, the results showed that the doping process introduced impurities into the graphene structure that affected the product quality. The wet chemical doping of GO was also reported by different research groups, but in all of them the doping procedure consisted of different steps, and the quality of the final product was dramatically affected by the procedure [15,16]. As can be seen, the wet chemical doping procedure is a widely used method, because it is simple and effective, but this process demands some extra steps such as transferring the graphene to the alkali metal solution, soaking the graphene or GO in the solutions for some time, and drying the soaked samples [13,15]. These extra steps introduce defects in the graphene structure and affect the quality of the final products. Furthermore, in some cases, prolonged soaking time resulted in developing alkali metal particles or impurities on the graphene matrix that deteriorated the optical transparency of the graphene layer drastically [12]. Furthermore, there are no reports that present the dopants' impact on the substrate's electrochemical characteristics. If the doped graphene coating is going to act as a low work function cathode on the metal substrate, the inertness of the coating could be one of the concerns that could be controversial in long term applications.

In fact, and beside its potential application in electronic devices, the chemical inertness, thermal stability (higher than 1500 °C under an inert environment), excellent mechanical properties, and water impermeability of graphene (thanks to its sp^2 orbital hybridization that forms a natural diffusion barrier) made it an attractive candidate in corrosion barrier field [17]. Since the graphene coating does not change the thickness and appearance of the substrate, it is an ideal coating to protect a metal substrate from the destructive effects. Many reports proved the potential of graphene as corrosion [2,18,19] and oxidation [20] barrier on different metal substrates. Especially chemical vapor deposition (CVD)-grown graphene coatings have been shown to significantly improve the corrosion resistance of copper, nickel, aluminum, and molybdenum [18,19,21–23]. Furthermore, the graphene coating doped with nitrogen (as an n-dopant) was also reported as a practical approach for improving the corrosion protection of metal via graphene coating [24,25], therefore, investigating the effect of the Cs (as an n-dopant) on the inertness of the G/Cs coating can be interesting.

Here we present experimental results on the effect of doping graphene with cesium, which has the lowest work function among the different alkali metals. We propose an improved CVD method instead of the wet chemical doping process with Cs_2CO_3, widely used in the past for doping graphene. Aside from being a simple one-step process, CVD is less time-consuming and provides a coating with a low level of impurities. In the process of synthesizing graphene via the CVD method, Cs_2CO_3 was introduced in the furnace and thermally evaporated, which resulted in doping of the growing graphene layer. A detailed characterization study with X-ray photoelectron spectroscopy (XPS) and Raman spectroscopy revealed that graphene was successfully doped with Cs. As anticipated, due to the low work function of Cs, the work function of the graphene layer was lowered.

Different electrochemical techniques were used to investigate the effect of the dopant on the chemical inertness of the graphene layer and determine the effect of Cs on corrosion susceptibility of graphene coating on copper in 0.1 M NaCl solution.

2. Experimental

2.1. *Materials*

The reaction gases, methane (CH_4, with 99.995% purity), hydrogen (H_2, 99.999%), and argon (Ar, 99.999%) were obtained from A-Rang Gas, Korea. A 0.254 mm thick Cu (99.95%) foil was purchased from Alfa Aeser, USA. Cs_2CO_3 (99.994%) was purchased from Alfa Aeser, UK. The thermal CVD equipment, purchased from Scientific Engineers (S. Korea), was used to deposit graphene coating on the Cu foils. NaCl (Sigma Aldrich, USA) and deionized water from the Milli-Q system (Millipore, USA) were used in all electrochemical experiments.

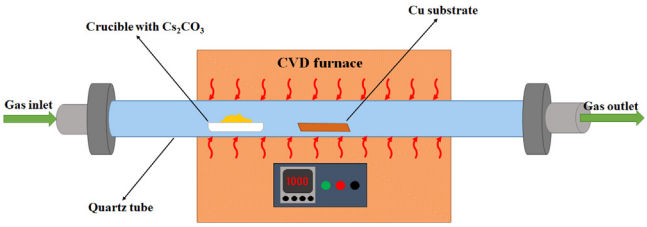

Fig. 1 – Schematic illustration of the doping process during CVD of graphene.

2.2. CVD of graphene and cesium-doped graphene (G/Cs) on copper substrate

The CVD method was utilized as a synthesis method for depositing G/Cs coating on Cu foil as the catalyst ($1 \times 1\,cm^2$ and $2.5 \times 2.5\,cm^2$). After the pre-annealing process (Supporting information), Cs_2CO_3 (as Cs precursor) was introduced into the tube furnace along with the Cu substrate. The tube furnace temperature increased from room temperature to 1000 °C, while the samples were exposed to H_2/Ar (200/200 sccm). After reaching 1000 °C, the samples were kept at this temperature for 20 min, then exposed to the CH_4/H_2/Ar gas mixture (100, 200 and 200 sccm, respectively) for 10 min and then the furnace was cooled to room temperature (100 °C/min cooling rate) under the same starting gas mixture employed in the heating step. A past study showed that heating Cs_2CO_3 up to 600 °C results in the decomposition of this material [26]. Therefore the presence of this material in the tube furnace during the graphene growth resulted in doping of the graphene layer with Cs dopants (Fig. 1). The pure graphene coating was grown in a similar synthesis procedure without introducing the Cs_2CO_3 into the feedstock. Since the length of the hot zone in the CVD furnace was limited and to make sure of the reproducibility of the doping technique, every time 3–4 samples (based on their sizes) were prepared.

2.3. Characterization

To investigate the morphological characteristics of the samples, scanning electron microscopy (SEM, Stereoscan 440 from Leica/Cambridge) was utilized. X-ray photoelectron spectroscopy (XPS) was used to evaluate the chemical compositions of the coatings. XPS was performed using a K-Alpha System (Thermo electron) spectrometer equipped with AlK_α monochromatic X-ray source (1486.7 eV) and a micro-focused monochromator. The pass energy was 200 eV for the survey spectra and 50 eV for the high-resolution spectra. The quality of the obtained samples and their doping procedure were investigated using Raman spectroscopy (RFS 100/S, Bruker, $\lambda = 532$ nm, resolution $1\,cm^{-1}$). The work function was obtained by ultraviolet photoelectron spectroscopy (UPS) technique (UPS, R4000 spectrometer, VG scienta, UK). The chemical composition of the samples before and after 15-day immersion in 0.1 M NaCl was investigated using LEO SUPRA 55 (Carl Zeiss AG, Germany), equipped with an energy-dispersive X-ray spectroscopy (EDX) instrument EDAX GENESIS 2000 (EDAX Inc., USA).

2.4. Electrochemical measurements

The corrosion stability of bare Cu, graphene-coated Cu (G-Cu), and G/Cs-coated Cu (G/Cs-Cu) was monitored in 0.1 M NaCl for 15 days. Three-electrode setup was employed, including the bare Cu or graphene-coated Cu, and G/Cs-coated Cu, Pt mesh, and saturated calomel electrode (SCE) serving as working, counter and reference electrodes, respectively. All potentials were reported versus SCE. Electrochemical tests were carried out with the Reference 600 instrument (Gamry, USA). Open circuit potential, E_{OCP}, was monitored for at least 30 min before each measurement to ensure satisfactory stability. The electrochemical impedance spectroscopy (EIS) was performed with 5 mV sinusoidal AC voltage variation around E_{OCP}, over the 100 kHz-10 mHz frequency range. Echem Analyst software (Gamry, USA) was used for impedance spectra fitting and analysis. Polarization measurements were carried out after 15-day immersion in 0.1 M NaCl using both linear polarization (±15 mV vs. E_{OCP}, $0.125\,mV\,s^{-1}$ scan rate) and potentiodynamic sweep (±150 mV vs. E_{OCP}, scan rate $0.5\,mV\,s^{-1}$) techniques.

3. Results and discussion

3.1. Scanning electron microscopy (SEM)

SEM images of bare Cu film before pre-treatment and coating deposition showed imperfections, cracks, and a rough texture, which were the characteristics of cutting and cold rolling processes (Fig. 2a). The impurities and metal oxides on the bare Cu can be another reason for these morphology imperfections. After depositing graphene on the Cu foil, which was accompanied by a pre-treatment process, the oxide layers on the Cu surface were removed. Due to the high growth temperature of graphene (1000 °C), melting the surface of the Cu substrate can also bring surface reconstruction of Cu that significantly affected the surface morphology and resulted in a smoother surface compared to the bare Cu foil (Fig. 2b). In order to grow a defect-free graphene layer, pre-treatment of the Cu foil is mandatory. The metal oxides and impurities on the Cu surface act as obstacles for the growth of a continuous graphene layer and provide nucleation sites for mono- and bi-layer graphene growth. The pre-treatment steps greatly improved the Cu substrate's imperfections, and the rough and non-uniform morphology of the Cu substrate before pre-treatment was changed after pre-treatment to a perfectly soft and uniform surface that is needed for graphene growth. Therefore, the Cu foil's pre-treatment process before the growth of graphene and etching the Cu surface via H_2 at a high temperature (1000 °C) in the CVD furnace seems a mandatory step to have a high-quality graphene layer. The SEM images of the graphene-coated samples showed a uniform surface. For the G/Cs-coated sample (Fig. 2c), compared to the bare Cu foil, a uniform smooth surface was observed, and there was no sign of particle or agglomeration on the surface, which can be a sign of homogenous distribution of the Cs elements on the sample.

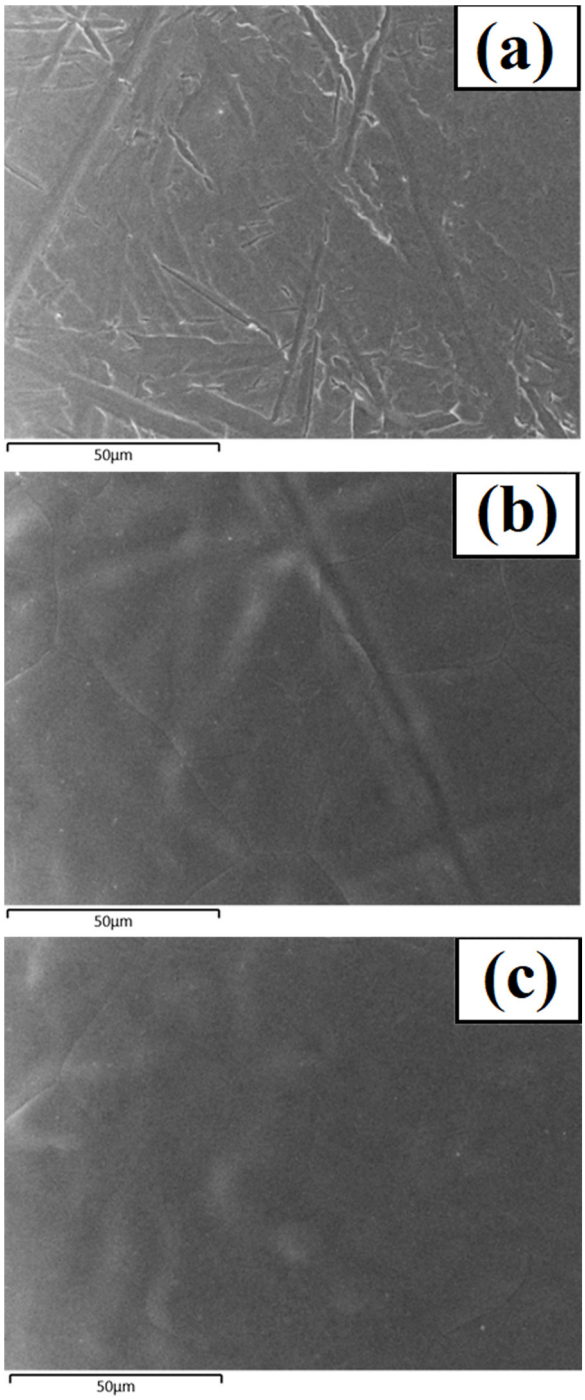

Fig. 2 – SEM images of (a) bare Cu, (b) graphene-coated Cu, and (c) G/Cs-coated Cu foil.

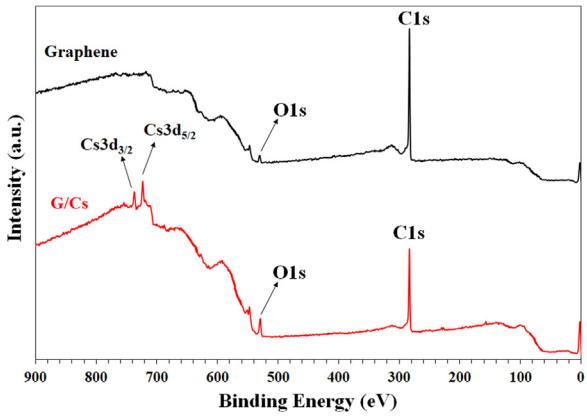

Fig. 3 – The XPS survey scan data of graphene coating and G/Cs coating.

3.2. *X-ray photoelectron spectroscopy (XPS)*

XPS provides useful information on the doping process of the graphene coating during the CVD procedure, as well as the chemical composition of the samples. The XPS survey spectra of the graphene coating and G/Cs coating are presented in Fig. 3. The G/Cs spectra have pronounced Cs peaks ($Cs3d_{3/2}$, $Cs3d_{5/2}$), indicating the presence of Cs element along with the other elements on the substrate. Based on the information regarding the chemical composition of the graphene coating and G/Cs coating, the elements presented on the surface were C and O for graphene coating and C, O, and Cs for the G/Cs coating. In comparison with the C1s peak of pure graphene coating (284.5 eV), there is a small shift of C1s peak of the G/Cs coating (285.1 eV) to the higher binding energy, supporting the assumption of the electron transfer between the graphene coating and Cs, and n-type doping of graphene coating [12]. Although the bare Cu foils underwent pre-treatment to remove the remnant oxide from their surface before CVD, a small amount of oxide can be observed on the surface after the coating deposition. Since the CVD method was at ambient pressure, the presence of oxide in the tube furnace during the deposition process can be one of the reasons for observing O element in the coatings' composition.

Fig. 4a and b shows the deconvoluted C1s XPS spectra of pure graphene coating and G/Cs coating, respectively, with peaks assigned to different functional groups. Corrections due to charging effects were performed with respect to C1s at 284.5 eV, and all spectra underwent a Shirley background subtraction before curve fitting. Generally, the C1s peak of pure graphene coating contains four different carbon bonds such as C=C bond (sp^2 hybridized carbon) at about 284.5 eV, C—C bond (sp^3 hybridized carbon) at 285.4 eV, C—O bond at 286.6 eV, and a peak at around 288.5 eV assigned to carbonyl C=O group [27]. The intensity of the peak that originated from the sp^2-hybridized C is higher than the other peaks for both samples (Fig. 4a and b), indicating that both the graphene coating and G/Cs coating have a high graphitization degree. The oxygen-containing functional groups in the C1s XPS spectra of the samples might have originated from the remnant oxygen adsorption in the tube furnace or the ambient O_2 adsorption after the samples were removed from the reaction chamber.

Fig. 4c and d shows the high-resolution XPS spectra of the O1s region for both graphene coating and G/Cs coating. Four peaks resulted from the deconvolution of the O1s core-level spectrum. The peaks at about 529.4 eV are related to the CuO phase (cupric oxide), whereas the 530.2 eV peak was attributed to Cu_2O phase (cuprous oxide){Barreca, 2007 #172}. The rela-

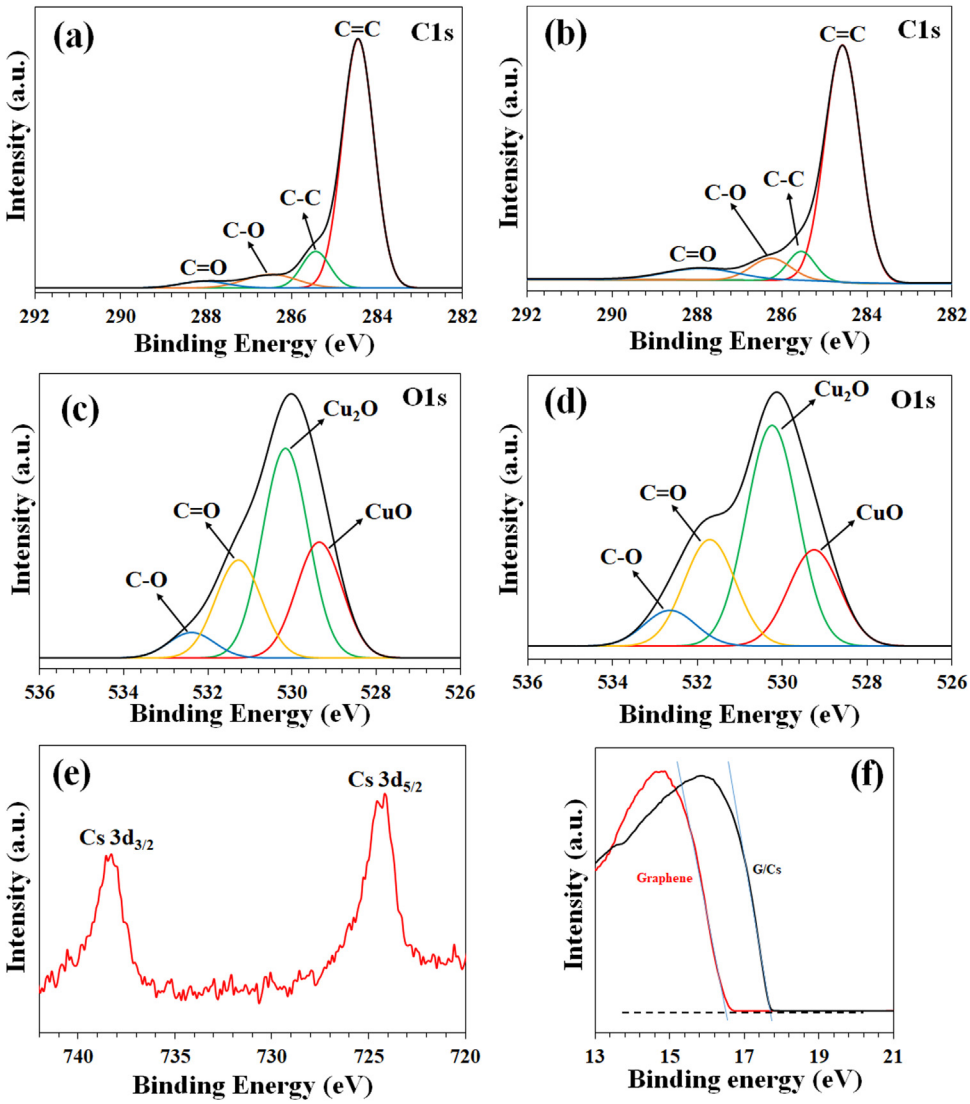

Fig. 4 – XPS C1s spectra of (a) graphene coating and (b) G/Cs coating; O1s spectra of (c) graphene coating and (d) G/Cs coating; (e) Cs3d spectra of G/Cs coating, and (f) UPS spectrum (the cutoff region) of the graphene and G/Cs.

tive percentages of CuO and Cu_2O phases, calculated based on measured peak areas, were 25.8% and 46.7% (G-Cu), and 21.0% and 48.1% (G/Cs-Cu), respectively. By comparing the composition of these two phases for graphene coating and G/Cs coating, it can be seen that for the graphene coating CuO phase has higher concentration (25.8%) than CuO phase in G/Cs coating (21.0%), while the Cu_2O phase of graphene coating has lower concentration (46.7%) than the same phase in G/Cs coating (48.1%). Based on the previous report, the Cu_2O is an unstable oxide phase that can easily turn to CuO in the presence of oxygen [28]. During the ambient pressure CVD, the oxygen inside the CVD chamber affected both coatings and substrates during the deposition. Apparently, in the case of graphene coating, the amount of oxygen that reached the substrate was higher than G/Cs; therefore, the concentration of CuO is higher in the case of graphene coating. O1s XPS analysis showed that the concentrations of C=O (531.3 eV) and C—O (532.4 eV) were higher (23.2 % and 7.7 %, respectively) in G/Cs coating than in graphene coating (21.9 % and 5.6 %, respectively).

Fig. 4e presents the Cs3d peaks of Cs, where smaller binding energy of $Cs3d_{5/2}$ in G/Cs coating (724.4 eV) can be observed as compared to the one reported in the literature (726.4 eV) [29]. Based on the reports, this shift implies the existence of additional positive charges surrounding the Cs atoms, which could be due to the electron transfer from Cs to graphene coating [30].

3.3. *Ultraviolet photoelectron spectroscopy (UPS)*

Ultraviolet photoelectron spectroscopy was used to investigate the changes in the graphene work function by introducing cesium into its structure. UPS spectra were obtained using the He I irradiation ($h\nu = 21.2$ eV). To avoid interference of the spectrometer threshold in the UPS spectra, samples were biased at −10 V during UPS measurements and observed the secondary

electron edge. The work function of the sample W is computed as:

$$W = h\nu - (E_F - E_{cutoff}) \quad (1)$$

where $h\nu$ is the photon energy of the excitation light (21.2 eV), E_F is the Fermi edge, and E_{cutoff} is the inelastic high binding energy cutoff. Fig. 4f shows the results of the UPS measurement (cutoff region) of graphene and G/Cs samples. As shown in Fig. 4f, the cutoff binding energy of graphene is 16.7 eV. According to Eq. (1), the average measured values for a work function of 3 different graphene samples were about 4.5 eV, which was in agreement with previously reported values for graphene [31]. By doping graphene with cesium, the cutoff binding energy shifted about 1.2 eV to higher binding energies, and the work function of G/Cs was reduced to 3.3 eV. Therefore, doping graphene with n-doping agents (electropositive elements) increases its electron density and lowers its work function.

3.4. *Raman*

Raman spectroscopy is known as a useful and non-destructive method that has been utilized to characterize the number of layers, the quality of graphene coating, and the presence of defects and disorders. Furthermore, this method is very sensitive to doping. In the Raman pattern of ideal single-layer graphene (without any defects), the G band (at around 1570–1585 cm^{-1}) and 2D band (at around 2640–2680 cm^{-1}) are the predominant features. On the other hand, the presence of defects and disorders results in the appearance of some other peaks, such as D band (at around 1320–1350 cm^{-1}), D' band (at around 1602–1625 cm^{-1}), G* band (at around 2460 cm^{-1}), and D + G band (at around 2940 cm^{-1}). In a Raman pattern (starting from the lower wavenumbers) first, there is the D band that is activated by defects and is due to the breathing modes of sp^2 rings [32]. Since the intensity of the D band is strongly associated with the degree of disorder of graphene, the absence of the D band will guarantee the excellent crystallization of the graphene coating. The G band originates from the first-order Raman scattering process and corresponds to the primary in-plane vibrational mode of sp^2 carbon atoms. The intensity of this peak will increase linearly with increasing graphene coating thickness because more carbon atoms are detected in the multi-layer graphene [33]. If there are some randomly distributed impurities, domain boundaries, or graphene edges, the G-peak can split into two peaks, G peak (1580 cm^{-1}) and D′ peak (1620 cm^{-1}) [32]. If there is a short-range disorder (e.g., defects, adatoms, or vacancies), a D band would be observed in the Raman pattern of graphene, while long-range disorders (charged impurities, ripples, or dislocations) would introduce a D′ band into the graphene Raman pattern. The D′ band arises from the double resonance, intravalley, defect-induced, process [32]. The G* band appears in the Raman pattern that originates from a combination of the in-plane transverse optical phonon and the zone boundary in-plane longitudinal acoustic phonon modes [34]. The 2D band originates from a two-phonon double resonance process. It is an overtone of the D band and always appears in the graphene Raman spectrum even when its first order is absent. The shape and position of the 2D band are related to the number of graphene layers, and this peak becomes broad and upshifts when the number of graphene layers increases from a single-layer to multi-layer graphene [32]. Moreover, the last feature in the Raman pattern of graphene (consisting of defects and disorders) is a combination scattering mode D + G band (at around 2950 cm^{-1}), which requires abundant edges and defective sites for its activation.

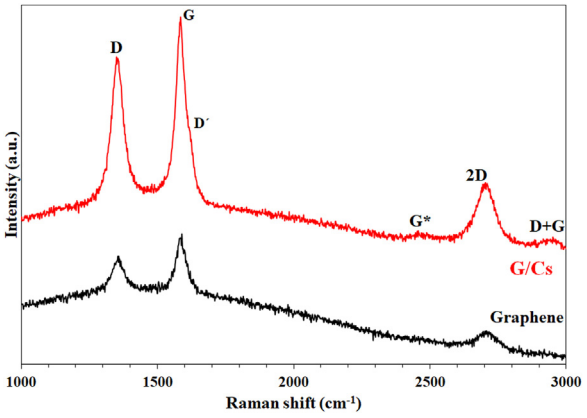

Fig. 5 – Raman patterns of graphene coating and G/Cs coating.

As can be seen in Fig. 5, pure graphene coating only contained D, G, and 2D bands, while after doping, some other bands (D′, G*, and D + G) appeared in the Raman pattern. The D band was present in both samples, corresponding to the low crystallinity of the graphene coatings, which is typical for CVD of graphene at ambient pressure. The intensity of D, G, and 2D bands (I_D, I_G, and I_{2D}) provides useful information about the structure of the synthesized graphene coating. From the intensity of the peaks in Fig. 5, it can be observed that the I_D/I_G ratio of pure graphene coating is smaller than that of G/Cs coating (0.53 to 0.69, respectively), demonstrating that doping graphene with Cs atoms deteriorates the quality of the graphene coating and increases the number of defects and edges in its structure. Moreover, the I_D/I_G ratio is inversely proportional to the graphene domain size, L_α, which shows that increasing the number of defects will reduce the domain size of the graphene coating (Eq. (2)). The L_α is related to the graphene coating's domain size (or average distance between defects) and can be calculated using the I_D/I_G intensity ratio and the Tuinstra–Koenig relation [35]:

$$L_\alpha = 2.4 \times 10^{-10} \lambda_{laser}^4 \left(\frac{I_D}{I_G}\right)^{-1} \quad (2)$$

where L_α is the graphene domain size (in nm), and λ_{laser} is the excitation laser wavelength (532 nm). The doping process is usually accompanied by introducing defects and edges into the graphene coating structure. After Cs-doping of graphene coating, the I_D/I_G increases from 0.53 to 0.69, which means the domain size is smaller for G/Cs coating than pure graphene coating (27.8 nm and 36.2 nm, respectively). Smaller domain size (or grain size) of the G/Cs coating implies the presence of more grain boundaries in the coating's structure. The grain boundaries can act as a site for electron scattering,

which negatively affects the electron transport of the coating and degrades the coating's electrical conductivity and carrier mobility [12,13]. Further, the change in grain size and the presence of the grain boundaries could also affect the material's electrical properties [36–38], including conductivity [39].

Apart from I_D/I_G, another useful method for investigating the characteristics of graphene is the intensity ratio of 2D to G bands (I_{2D}/I_G) that is dependent on the number of graphene layers. It is known that $I_{2D}/I_G \geq 2$ refers to single-layer graphene (SLG); $I_{2D}/I_G < 1$ refers to few-layer graphene (FLG), while $1 < I_{2D}/I_G < 2$ refers to bi-layer graphene (BLG) [18]. Based on the G and 2D band intensities (I_G and I_{2D}) extracted from the Raman spectrum in Fig. 5, graphene coating shows higher I_{2D}/I_G than G/Cs coating (0.43 and 0.31 respectively), which means that both coatings are FLG and the thickness of pure graphene coating is smaller than G/Cs coating.

The shifting of the G band in the Raman pattern provides additional information about the doping process. Some studies showed that the G band upshifts (higher wavenumber) via hole doping (p-dopant) or downshifts (lower wavenumber) via electron doping (n-dopant) [12,40], therefore in the case of Cs-doping (as an n-dopant), G band is expected to shift towards lower wavenumbers (downshift) [41,42]. Based on this information and considering the peak position G band in the Raman pattern of G/Cs coating (1577 cm^{-1}), a downshift of this band can be observed in comparison with pure graphene coating (1585 cm^{-1}) that implies the n-type doping of graphene coating [14]. Apart from the intensity and location of the peaks, the D band's full width at half-maximum (FWHM) is also changed by doping graphene layers via the Cs dopants. Previous studies showed that due to the bonding structure and the generation of new defects after doping, the widths of D bands get broader than pure graphene coating [43]. The FWHM of the D band for graphene coating is smaller than that for G/Cs coating (58 cm^{-1} and 62 cm^{-1}, respectively), indicating an increased number of defects in the graphene coating after doping process. Based on these results, it is concluded that the *in-situ* n-doping of graphene coating with Cs atoms was successful. However, the pure graphene coating composed of fewer layers, fewer defects, and larger domain size as compared to the G/Cs coating.

3.5. *Energy dispersive X-ray spectroscopy (EDX)*

Surface composition and elemental analysis of the bare Cu, graphene-coated Cu (G-Cu), and G/Cs-coated Cu (G/Cs-Cu) samples before and after of exposure to 0.1 M NaCl were evaluated using EDX analysis (Table 1). All samples contained Cu and O (originating from the present oxides), along with C for graphene coating, and C and Cs for G/Cs coating. The bare Cu before exposure contains a small amount of oxygen, due to the exposure to ambient air. Pre-treatment of Cu film before graphene deposition and depositing graphene coating on Cu film at 1000 °C removed most of the oxide layer from the Cu surface. From Table 1, it can be seen that the Cu surface after graphene deposition still contains a negligible amount of oxygen. Since the graphene was deposited on the Cu substrate in an APCVD technique, the presence of oxygen in the tube furnace is undeniable, and it can be assigned to the oxidation of Cu foil through the defected sites of the graphene coating or graphene grain boundaries. Comparing the amounts of C in the composition of graphene coating (11.7 at.%) and G/Cs coating (15.5 at.%) showed a higher amount of C for G/Cs coating. Based on the Raman results (Section 3.4), the G/Cs coating was composed of more graphene layers compared to the graphene coating; therefore, higher carbon content in the EDX characterization could be due to this situation.

Table 1 – Surface element contents for bare Cu, G-Cu, and G/Cs-Cu samples, as-prepared and after 15 days of immersion in 0.1 M NaCl, determined by EDX analysis.

	Sample	Element content (at.%)			
		Cu	C	O	Cs
As prepared	bare Cu	97.0	–	3.0	–
	G-Cu	88.0	11.7	0.3	–
	G/Cs-Cu	82.5	15.5	1.0	1.0
15 days in 0.1 M NaCl	bare Cu	88.8	–	11.2	–
	G-Cu	82.9	12.4	4.7	–
	G/Cs-Cu	80.5	16.3	2.2	1.0

The EDX data after 15 days of immersion in 0.1 M NaCl (Table 1) indicated that the corrosion of the metal occurred for all samples, as evidenced by decreased Cu content. For bare Cu, the oxygen content increased significantly from 3.0 at.% to 11.2 at.%, indicating a high oxidation rate of the bare Cu surface. The increase in oxygen content could indicate the growth of a copper oxides layer, which may cause slight passivation of the Cu surface. The amount of O also increased for G-Cu (4.7 at.%) and G/Cs-Cu (2.2 at.%) samples, pointing to the growth of oxide layers on the Cu surface during immersion in 0.1 M NaCl. However, the O content after 15-day immersion was lower for G/Cs-Cu (2.2 at.%) in comparison with G-Cu (4.7 at.%). Specifically, the amount of O content was lower for as-prepared G-Cu (0.3 at.%), compared to G/Cs-Cu (1.0 at.%), which was reversed after 15 days of exposure to corrosion environment. Generally, EDX is not an infallible technique for quantification of trace amounts of elements, but the XPS also confirmed higher oxygen content for G/Cs-Cu (11 at.%) compared to G-Cu (2.5 at.%) for the as-prepared samples, so it is believable that the general trend observed by EDX was reliable. This change in oxygen content for the two coated samples after exposure to 0.1 M NaCl could be explained by forming a passive oxide layer in the coating pores, which was more pronounced for G-Cu. The formation of an oxide layer can help slow down the corrosion process if it acts as a passive barrier. This effect was hindered in the case of G/Cs-Cu, which could be explained by the property of the G/Cs coating to actually enhance corrosion and promote the dissolution of both the metal and the oxide layer, as will be shown through the electrochemical testing results in the following sections. The C and Cs contents for coated samples were almost unchanged after 15 days, confirming that there were no changes in the structures of coatings themselves. Further investigations of the corrosion behavior of different samples will be carried out using different electrochemical techniques in the following sections.

3.6. *Electrochemical impedance spectroscopy*

The impedance spectra for bare Cu (Fig. 6a and b), G-Cu (Fig. 6c and 6d) and G/Cs-Cu (Fig. 6e and f) showed decreasing trends of the overall impedance over the investigated 15-day period and consequently decreasing protective properties with exposure to the corrosion environment. However, even though the impedances for all of the samples decreased after 15 days (Fig. 6), the pure graphene-coated sample still possessed the highest impedance values compared to other samples, pointing to better protective properties of the pure graphene coating. G/Cs coating's Nyquist diagram underwent significant changes after 15 days, compared to day 0 (Fig. 6e), especially in the low-frequency region. This region is usually ascribed to the double layer on the metal/electrolyte interface, and the dramatic change in the shape and decrease of the overall impedance for G/Cs-Cu in this region could imply a decrease of the charge transfer resistance and enhanced corrosion of the metal under the coating. The appearances of Bode phase angle plots (Fig. 6b, d and f) are indicative of the presence of two time constants, RC, in the system, where one, at middle/higher frequencies depicts the coating and the other, at lower frequencies, illustrates the electrochemical double layer. For G-Cu (Fig. 6d), the reason for the appearance of one wide peak after 30 min and 7 h, instead of two separate, is the thin but compact graphene coating that was not significantly affected by the electrolyte upon short term immersion and there were not many pores through which the electrolyte could come in contact with the metal, so there was no sufficient interaction to obtain separate frequency-dependent responses of the graphene coating and the electrochemical double layer on the metal/electrolyte interface under the coating. This is also corroborated by the fact that the appearance of Bode diagrams (both the modulus and phase angle) did not significantly change between 30 min and 7 h. On the other hand, after 15 days, significant coating degradation has occurred, as also evidenced by the decreasing impedance values in the Nyquist plot in Fig. 6c and Bode modulus plot in Fig. 6d. This has led to the change in the phase angle responses of the graphene coating and the double layer on the electrode/electrolyte interface, depicted as two "peaks" in the phase angle plots. On the other hand, G/Cs-Cu (Fig. 6f) exhibited two separate peaks even initially (after 30 min and 7 h), indicating the poor initial coating quality that led to exposed large surface area of the metal and the significant response from the electrochemical double layer even upon short-term immersion, which is in line with poor anticorrosion performance of the G/Cs coating compared to pure G.

The impedance values for G-Cu were significantly higher than both bare Cu and G/Cs-Cu after 30 min (Fig. 7a and b) and 15 days (Fig. 7c and d) of immersion in 0.1 M NaCl. G-Cu even exhibited higher impedance after 15 days (Fig. 7c and d) compared to bare Cu after 30 min (Fig. 7a and b), indicating the superior anti-corrosion performance of G-Cu and the ability of graphene coating to inhibit the corrosion of copper significantly. On the other hand, G/Cs-Cu exhibited the lowest anti-corrosion performance of all investigated samples, even lower than bare Cu (insets in Fig. 7a and c). This behavior could be explained as follows. First, the adhesion of Cs-doped graphene coating on Cu substrate was lower compared to pure graphene coating on Cu (as determined by visual inspection of the coating surfaces, where flaking and delamination was observed for G/Cs coating, unlike the pure graphene coating), leading to incomplete coverage of the metal. The delamination and incomplete coverage of the metal by the G/Cs coating could play a significant role in coating's anti-corrosion performance. It is well known that graphene is highly conductive and could form a galvanic cell on the metal surface, leading to worsened corrosion stability of the coated sample, compared to the non-coated one [44]. This effect could be significant even though some studies have shown that the conductivity of graphene sheets could decrease after doping with alkali metals [12,45]. Thus, the Cs-doped graphene coating exposed anodic sites on the metal surface, promoting active dissolution of Cu and leading to decreased overall anti-corrosion performance. Another effect of n-doping of the graphene coating with Cs is reflected in lowering the electron work function, as determined by UPS measurements (Section 3.3). The lower work function of the G/Cs coating (3.3 eV) compared to pure graphene (4.5 eV) could have a profound effect on anti-corrosion performance. It is well known that lowering the surface work function would lead to enhanced copper corrosion, due to higher activity of electrons at the grain boundary [46–48]. Lowering the electron work function would cause the surface to become more electrochemically active [46], thus decreasing the corrosion resistance of copper, as observed for G/Cs-Cu samples. However, in order to verify the mechanism of Cs-doping influence on G/Cs coating's anti-corrosion performance, more in-depth studies should be carried out.

The obtained EIS spectra were fitted with equivalent electrical circuits (EEC) presented in Fig. 8, to elucidate the physical model of the metal surface and to obtain the time variations of corrosion parameters during exposure to 0.1 M NaCl.

Bare Cu sample was fitted with the EEC shown in Fig. 8a, where an ohmic electrolyte resistance, R_Ω, was connected in series to three parallel RC circuits. The first RC circuit depicted constant phase element, CPE_c, and pore resistance, R_p, of the oxide layer on the Cu surface, as confirmed by EDX analysis (Table 1). Moreover, the copper oxide species were determined by XPS (Section 3.2) using the deconvolution of the O1s, proving that the oxide layer on the Cu surface consisted of mixed CuO and Cu_2O oxides. Analyzing further the physical model of the bare Cu/electrolyte interface (represented schematically in Fig. 8a), we proposed that the second RC circuit with constant phase element, CPE_{dl}, and charge transfer resistance, R_{ct}, corresponded to the electrochemical reaction of Cu corrosion in the electrochemical double layer on the metal/electrolyte interface inside the pores of the oxide layer, as follows. The mechanism of the Cu corrosion reaction in the chloride-containing electrolyte can be described using Eqs. (3) and (4), where the first step is the oxidation of Cu to Cu^+ ions and instantaneous reaction with Cl– ions in the electrolyte, resulting in the formation of CuCl salt corrosion product (Eq. (3)) [49]. However, CuCl reacts almost immediately with the excess Cl– ions to form soluble $CuCl_2$– corrosion products (Eq. (4)), which then diffuse away from the interface into the bulk solution [49]. The third RC circuit at low frequencies (constant phase element, CPE_F, and resistance, R_F) was assumed to illustrate the faradaic redox processes involving corrosion products and/or dissolved oxygen, taking place at the electrode surface [50,51].

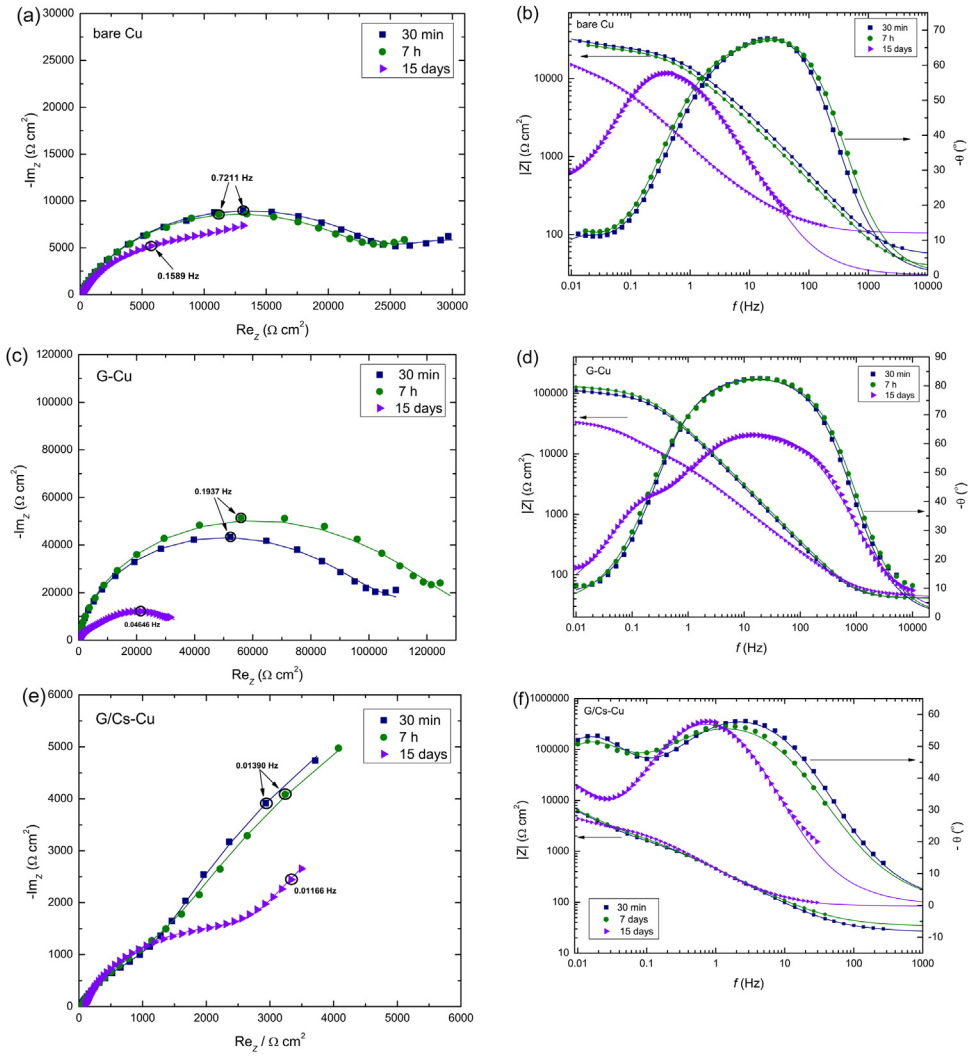

Fig. 6 – (a,c,e) Nyquist and (b,d,f) Bode plots of (a,b) bare Cu, (c,d) G-Cu and (e,f) G/Cs-Cu after different immersion periods in 0.1 M NaCl.

The rate of Cu corrosion in chloride media was proven to be under mixed control; i.e., it is controlled by both charge transfer and mass transport which is thought to be directly related to the diffusion of $CuCl_2$– ions that formed in reaction (4) away from the electrode surface [49]. Thus, the $CuCl_2$– corrosion products can participate in redox reactions at the metal/electrolyte interface, giving rise to the faradaic capacitance and resistance elements [50]. The goodness of fit (χ^2) parameter was of the order of magnitude of $\sim 10^{-6}$ for bare Cu spectra.

$$Cu + Cl^- \rightarrow CuCl + e^- \quad (3)$$

$$CuCl + Cl^- \rightarrow CuCl_2^- \quad (4)$$

On the other hand, G-Cu and G/Cs-Cu were fitted with an EEC presented in Fig. 8b, where CPE_C represented a constant phase element of G or G/Cs coating and oxide layer, whereas R_p was used to describe the G or G/Cs coating pore resistance and oxide layer resistance. Both the oxide layer and the G or G/Cs coating were assumed to be very thin (the thickness of the G and G/Cs coatings was confirmed to be only a few atomic layers, as discussed in the Raman spectroscopy (Section 3.4)), therefore they were represented as one time constant instead of two. The CPE_{dl} and R_{ct} circuit elements described the electrochemical double layer on the electrode/electrolyte interface in the oxide layer's pores and coating's top layer (Fig. 8b). However, in this case, there was no RC circuit depicting the faradaic redox processes, as the thicker top layer (G or G/Cs coating + the oxide layer) was assumed to suppress the effect of faradaic contributions. The goodness of fit (χ^2) parameter was of the order of magnitude of $\sim 10^{-6} - 10^{-3}$ for both G-Cu and G/Cs-Cu spectra.

The time dependences of calculated resistances and capacitances are presented in Fig. 9. The impedance of a CPE element (Z_{CPE}) can be represented with the following equation [52]:

$$Z_{CPE} = Y_0^{-1}(i\omega)^{-n} \quad (5)$$

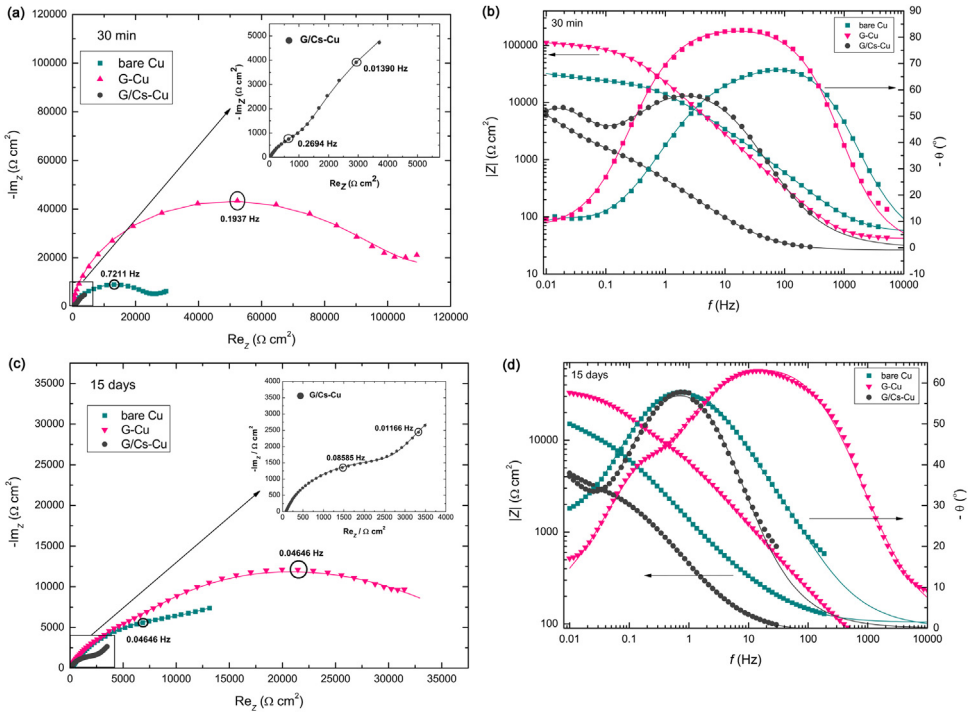

Fig. 7 – Comparison of impedance spectra for bare Cu, G-Cu and G/Cs-Cu after (a, b) 30 min and (c, d) 15 days of immersion in 0.1 M NaCl.

where $i^2 = -1$, Y_0^{-1} is CPE admittance, and ω is the angular frequency. The parameter n describes the deviation of CPE from a pure capacitor ($n = 1$), while for $n = 0$, it would become a pure resistor. The capacitance, C_{CPE}, of a CPE element in the non-ideal case, can be calculated from Eq. (6) [52], where ω_{max} is the angular frequency of a semicircle maximum on the imaginary axis in the complex plane.

$$C_{CPE} = Y_0(\omega_{max})^{n-1} \quad (6)$$

However, when the values of n are larger than 0.8 or close to 1.0, the capacitance can be approximated with Y_0, which was done in our case, as the n values were in the range 0.8–1.0.

From the obtained curves, it is evident that both R_p (Fig. 9a) and R_{ct} (Fig. 9b) values exhibited decreasing trends over the 15 days. G-Cu sample exhibited the highest values of both coating pore resistance and charge transfer resistance, pointing to superior anti-corrosion performance of the graphene-coated copper. Interestingly, the R_p values for G/Cs-Cu increased ever so slightly during the 15 days, possibly due to the growth of a mixed CuO/Cu_2O layer. On the other hand, R_{ct} for this sample steadily decreased up to day 15, confirming the progressing corrosion of Cu and poor protective properties of Cs-doped Gr coating. Similarly, the R_p for bare Cu increased up to around 8 days, due to the growth of a passive oxide layer on the metal surface and then decreased with the exposure time.

The time-dependent behavior of the monitored capacitances agreed with the observed resistance trends. The coating capacitance, C_c (Fig. 9c), increased as expected during immersion, and its values were lowest for the G-Cu sample. Similar behavior was also observed for double-layer capacitance, C_{dl} (Fig. 9d), that increased as corrosion intensified during 0.1 M NaCl exposure. G/Cs-Cu sample exhibited the highest values of both C_c and C_{dl} over the entire monitored period, evidencing the lowest protective properties of the Cs-doped graphene coating. The R_F behavior for bare Cu followed the general trend of the R_{ct} element, i.e., a slight increase after 24 h, followed by a sharp decrease until 4 days of immersion, and steadying off towards the end of the monitored 15-day period (Fig. 9e). This R_F decrease was followed by the increase in faradaic capacitance values, C_F, and this observed behavior could indicate progressing of Cu corrosion during 15 days in chloride media, as the formation of new corrosion products and their more intense redox reactions at the metal surface would lead to the increase in faradaic current flow, and therefore the decrease of the faradaic resistance and faradaic capacitance increase. It should also be noted that the parameter n for the CPE_F element was almost or even exactly equal to 1.0 during the entire period, indicating the almost pure capacitive nature of this element.

EIS measurements proved better protective properties of the graphene coating (G-Cu), as confirmed by the highest R_p and R_{ct} values (Fig. 9), as well as the highest impedances over the entire monitored period. On the other hand, the Cs-doped graphene coating (G/Cs-Cu) did not exhibit expected protective properties. It possessed even lower anti-corrosion performance than bare Cu foils (as shown by lowest impedances of G/Cs-Cu sample in Figs. 6 and 7), presumably due to poorer overall quality and lower work function of the n-doped graphene coating, as shown by Raman spectroscopy and UPS (Sections 3.3 and 3.4).

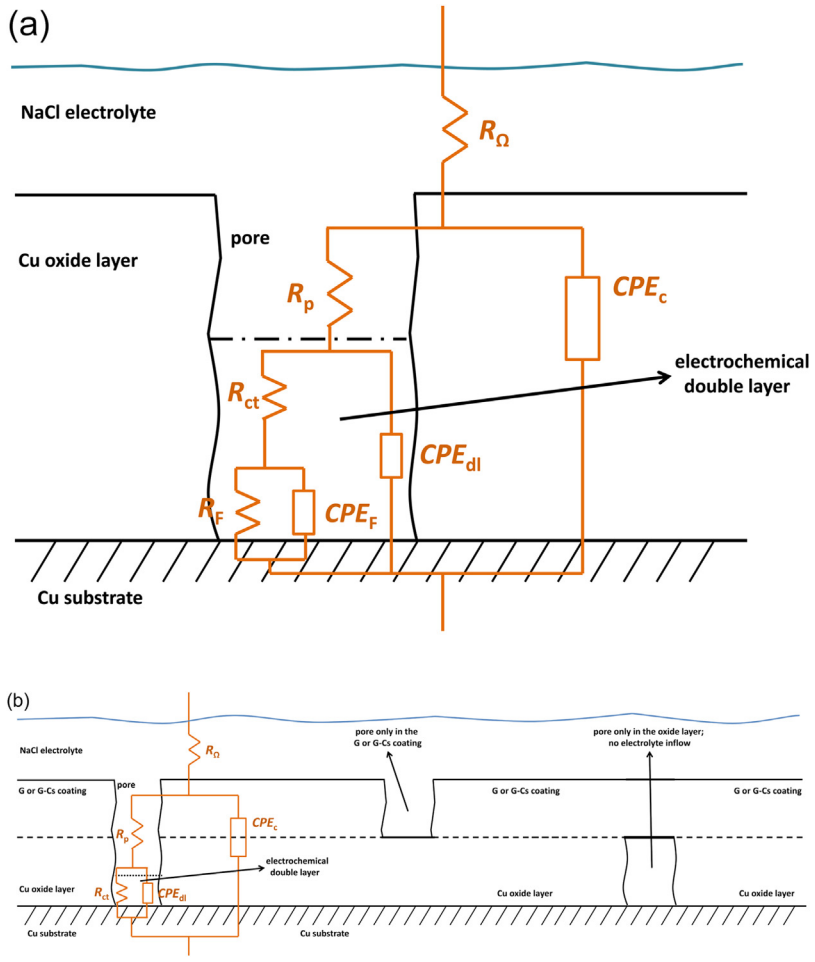

Fig. 8 – Equivalent electrical circuits used for EIS spectra fitting overlaid over schematic representations of surfaces and interfaces for (a) bare Cu and (b) G-Cu and G/Cs-Cu.

3.7. *Polarization measurements*

The potentiodynamic polarization curves (Fig. 10), recorded after 15 days of exposure to 0.1 M NaCl, provided qualitative and quantitative confirmation of EIS conclusions. The corrosion potentials, E_{corr}, corrosion current densities, j_{corr}, and anodic and cathodic Tafel slopes, b_a and b_c, were calculated by Tafel analysis of the obtained polarization curves, and their values are presented in Table 2. The G-Cu sample exhibited the lowest corrosion current density values (0.11 μA cm^{-2}), confirming the best corrosion protection properties of pure graphene coating on copper. On the other hand, G/Cs-Cu exhibited almost three times higher j_{corr} (0.65 μA cm^{-2}), compared to bare Cu (0.27 μA cm^{-2}), confirming the previous conclusion that the Cs-doped coating not only does not inhibit Cu corrosion but even enhances it. Linear polarization measurements also confirmed this behavior, as the calculated polarization resistance, R_{pol}, values (Table 2) were much higher for G-Cu (43.1 kΩ cm^2), compared to bare Cu (25.2 kΩ cm^2). In contrast, G/Cs-Cu exhibited the lowest R_{pol} values (17.1 kΩ cm^2), indicating better corrosion protection performance of the pure graphene coating than Cs-doped graphene coating.

From the appearance of bare Cu and G/Cs-Cu polarization curves (Fig. 10), it is evident that the mechanism and rate of the anodic reaction did not change between these two samples, indicating that G/Cs-Cu accelerated the Cu corrosion by influencing the rate of the cathodic reaction. The cathodic reaction during copper corrosion in aqueous media is believed to be an oxygen reduction reaction (ORR) [49,51]:

$$O_2 + 2H_2O + 4e^- \rightarrow 4\,OH^- \quad (7)$$

This reaction could also be written slightly differently, which is more appropriate in neutral to slightly acidic media:

$$O_2 + 4H^+ + 4e^- \rightarrow 2H_2O \quad (8)$$

Either way, the cathodic Tafel slope was the same for both bare Cu and G/Cs-Cu with the value of −100 mV dec^{-1} (Table 2), so we could assume that Cs-doped Gr coating did not influence mechanism of ORR, instead only accelerating its rate. The b_c value slightly decreased to −80 mV dec^{-1} in the case of G-Cu (Table 2), indicating that pure Gr coating could act as a corrosion barrier by changing the mechanism of the cathodic reaction. The anodic Tafel slopes were unchanged for all three samples (Table 2) and always close to 60 mV dec^{-1}, suggesting

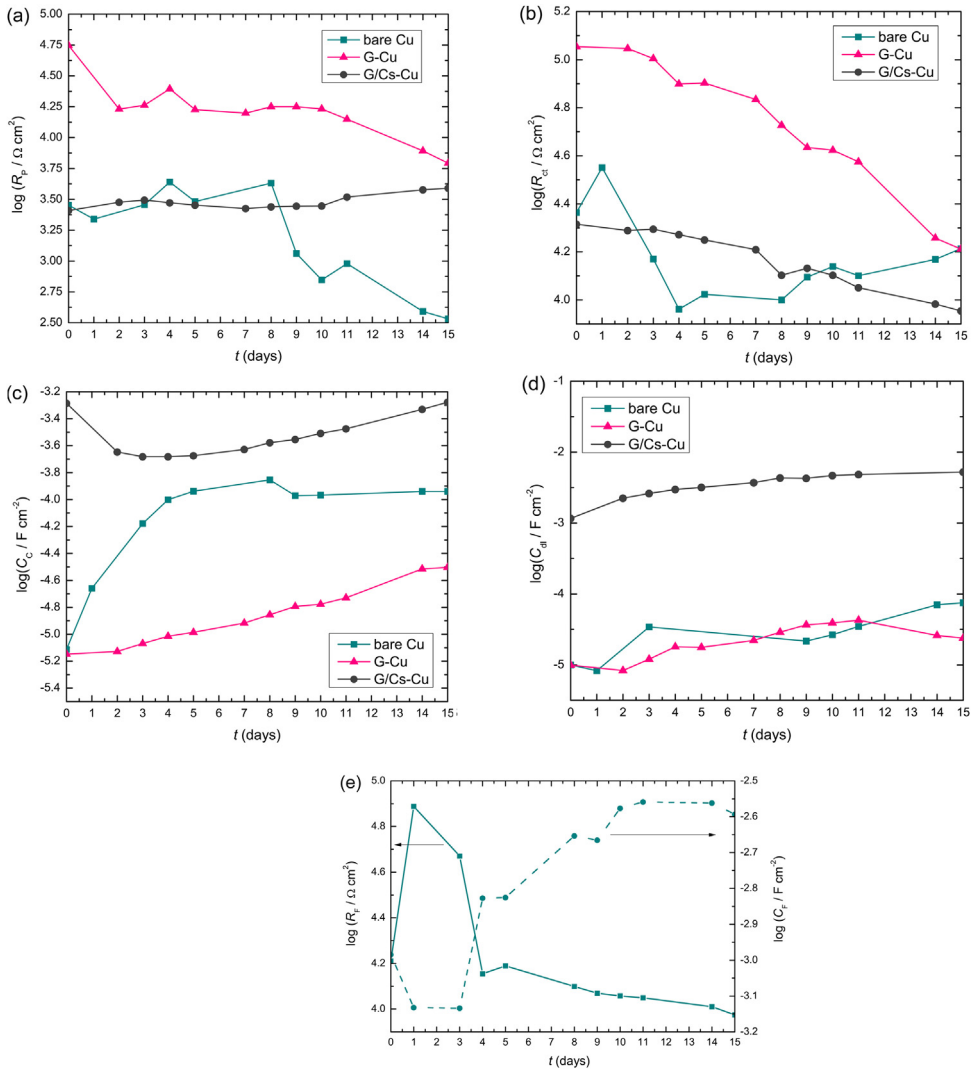

Fig. 9 – Time dependences of (a) R_p, (b) R_{ct}, (c) C_c and (d) C_{dl} for bare Cu, G-Cu and G/Cs-Cu, and (e) R_F and C_F for bare Cu during 15 days of immersion in 0.1 M NaCl.

Table 2 – Corrosion parameters for bare Cu, G-Cu and G/Cs-Cu calculated from polarization measurements after 15 days of immersion in 0.1 M NaCl.

	E_{corr} (mV vs. SCE)	j_{corr} (μA cm^{-2})	υ_{corr} (nm yr^{-1})	R_{pol} (kΩ cm^2)	b_a (mV dec^{-1})	b_c (mV dec^{-1})
Bare Cu	−182	0.27	6.26	25.2	62	−100
G-Cu	−150	0.11	2.55	43.1	60	−80
G/Cs-Cu	−156	0.65	15.1	17.1	65	−100

that the anodic reaction takes place through the usual mechanism, as described by Eqs. (3) and (4) above. This is also in accordance with anodic Tafel slope data from other studies [49,51].

The corrosion rates (υ_{corr}) of bare Cu, G-Cu and G/Cs-Cu were calculated from the obtained j_{corr} values, according to the Eq. (9), derived from the Faraday's law of electrolysis, where M(Cu) is the molar mass of copper (63.55 g mol^{-1}), ρ(Cu) is copper density (8.96 g cm^{-3}), z is the number of electrons exchanged in the copper corrosion reaction (Eq. (2)), and F is Faraday's constant (96,485 C mol^{-1}). The obtained corrosion rates (Table 2) were 6.26 nm yr^{-1} for bare Cu, 2.55 nm yr^{-1} for G-Cu, and 15.1 nm yr^{-1} for G/Cs-Cu, confirming that the G-Cu sample exhibited the best anti-corrosion performance.

$$\upsilon_{corr} = j_{corr} \cdot \frac{M(Cu)}{z \cdot F \cdot \rho(Cu)} \quad (9)$$

Such low corrosion resistance of G/Cs-Cu, compared to bare Cu and especially G-Cu, could be explained by the doping of the graphene with Cs atoms, which caused G to become n-type doped semiconductor [53], and therefore could have increased its electrical conductivity. On the other hand, as discussed above, there is some evidence that doping graphene with alkali metals (as opposed to, e.g., nitrogen doping [54])

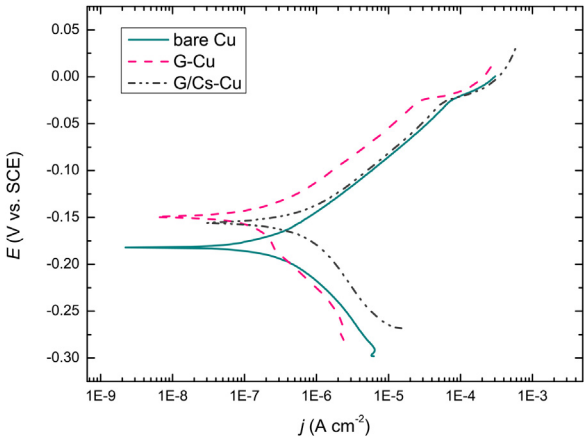

Fig. 10 – Polarization curves of bare Cu, G-Cu and G/Cs-Cu after 15 days of immersion in 0.1 M NaCl.

could actually decrease its conductivity [12,45]. However, the main problem with the G/Cs coating could be poorer quality with more disorders and defects (as confirmed by Raman spectroscopy), compared to pure graphene. The poorer overall quality of the coating could, presumably, lead some areas of the bare metal to become exposed to the electrolyte. Moreover, the high conductivity of graphene (even if it was lower after doping) could cause the formation of (micro)galvanic cells and accelerate the corrosion of the metal.

Further, the lower work function of G/Cs coating (3.3 eV), compared to pure graphene (4.5 eV), could lead to an increase in electrochemical activity of the surface, as discussed in the EIS section. The G/Cs coating also had smaller grain size than pure graphene (as determined from Raman spectroscopy measurements), which could cause increase in grain boundaries density at the surface with enhanced electron activity due to the lower work function [46], and this could lead to increased corrosion rate of G/Cs-Cu sample, as observed by polarization measurements. These effects taken together could lead to a decrease in the anti-corrosion performance of the n-doped coating compared to the pure graphene one.

4. Conclusion

The results of XPS and Raman spectroscopy revealed that the proposed CVD method could be used to achieve successful Cs-doped graphene (G/Cs) coating on copper. As compared with other techniques used for Cs-doping, like wet chemical doping, this method is one step, simple, and yields a coating free of impurities. The n-type character of the coating was confirmed by the XPS and Raman results. Shifting of the C1s and $Cs3d_{5/2}$ peaks to higher and smaller binding energies, respectively, and also shifting of the G band of the Raman pattern of the G/Cs coating compared to the pure graphene were measured. Ultraviolet photoelectron spectroscopy was employed to study the work function of graphene and G/Cs that indicated the lower work function of G/Cs compared with the graphene coating, resulting from increased electron concentration of the graphene coating due to the Cs dopants. The work function was decreased from 4.5 eV to 3.3 eV, which is a similar drop to the one obtained with multi-steps methods in previous works. Although the graphene was successfully doped with Cs elements, the Cu substrate's electrochemical characteristics were negatively affected by the G/Cs coating. First, Raman spectroscopy showed that the pure graphene coating had fewer layers, fewer defects, and larger domain size than the G/Cs coating. These features are reliable indicators about the deterioration of the graphene coating against corrosion due to the Cs-dopant. Second, electrochemical testing during 15-day immersion in 0.1 M NaCl confirmed better anticorrosion performance of pure graphene coating as compared to G/Cs coating: a higher value of polarization resistance and lower value of corrosion current density (from polarization measurements), higher impedance, coating pore resistance, charge transfer resistance values, and lower coating capacitance and double layer capacitance values (from EIS measurements).

Conflicts of interest

The authors declare no conflicts of interest.

Acknowledgments

This work was supported by Agencia Estatal de Investigación (Ministerio de Ciencia, Innovación y Universidades of Spain, grant No.: ESP2017-82092-ERC (AEI)); SN work is supported by Comunidad de Madrid (Spain) (grant No.: 2018/T2IND/11352); GSA work is supported by the Ministerio de Ciencia, Innovación y Universidades of Spain (grant No.: RYC-2014-15357). The authors thank the National Research Foundation of the Ministry of Education, Republic of Korea (Basic Science Research Program grant No.: 2018R1A2B5A02023190) and Ministry of Education, Science and Technological Development of Serbia (Contract No. 451-03-68/2020-14/200135) for financial support.

Appendix A. Supplementary data

Supplementary material related to this article can be found, in the online version, at doi:https://doi.org/10.1016/j.jmrt.2020.06.091.

REFERENCES

[1] Long F, Yasaei P, Sanoj R, Yao W, Král P, Salehi-Khojin A, et al. Characteristic work function variations of graphene line defects. ACS Appl Mater Interfaces 2016;8:18360.
[2] Naghdi S, Jaleh B, Ehsani A. Electrophoretic deposition of graphene oxide on aluminum: characterization, low thermal annealing, surface and anticorrosive properties. Bull Chem Soc Jpn 2015;88:722.
[3] Naghdi S, Jaleh B, Shahbazi N. Reversible wettability conversion of electrodeposited graphene oxide/titania nanocomposite coating: investigation of surface structures. Appl Surf Sci 2016;368:409.
[4] Boukhvalov D, Katsnelson M. Chemical functionalization of graphene. J Phys Condens Matter 2009;21:344205.
[5] Ramesh S, Yadav HM, Karuppasamy K, Vikraman D, Kim H-S, Kim J-H, et al. Fabrication of manganese oxide@nitrogen

doped graphene oxide/polypyrrole (MnO_2@NGO/PPy) hybrid composite electrodes for energy storage devices. J Mater Res Technol 2019;8:4227.
[6] Hibino H, Kageshima H, Kotsugi M, Maeda F, Guo F-Z, Watanabe Y. Dependence of electronic properties of epitaxial few-layer graphene on the number of layers investigated by photoelectron emission microscopy. Phys Rev B 2009;79:125437.
[7] Boukhvalov D, Katsnelson M. Chemical functionalization of graphene with defects. Nano Lett 2008;8:4373.
[8] Childres I, Jauregui LA, Tian J, Chen YP. Effect of oxygen plasma etching on graphene studied using Raman spectroscopy and electronic transport measurements. New J Phys 2011;13:025008.
[9] Huh S, Park J, Kim YS, Kim KS, Hong BH, Nam J-M. UV/ozone-oxidized large-scale graphene platform with large chemical enhancement in surface-enhanced Raman scattering. ACS Nano 2011;5:9799.
[10] Naghdi S, Sanchez-Arriaga G, Rhee KY. Tuning the work function of graphene toward application as anode and cathode. J Alloys Compd 2019;805:1117.
[11] Naghdi S, Rhee KY, Hui D, Park SJ. A review of conductive metal nanomaterials as conductive, transparent, and flexible coatings, thin films, and conductive fillers: different deposition methods and applications. Coatings 2018;8:278.
[12] Kwon KC, Choi KS, Kim BJ, Lee J-L, Kim SY. Work-function decrease of graphene sheet using alkali metal carbonates. J Phys Chem C 2012;116:26586.
[13] Chang J-H, Lin W-H, Wang P-C, Taur J-I, Ku T-A, Chen W-T, et al. Solution-processed transparent blue organic light-emitting diodes with graphene as the top cathode. Sci Rep 2015;5:9693.
[14] Park I-J, Kim TI, Cho I-T, Song C-W, Yang J-W, Park H, et al. Graphene electrode with tunable charge transport in thin-film transistors. Nano Res 2018;11:274.
[15] Chen Y, Lin W-C, Liu J, Dai L. Graphene oxide-based carbon interconnecting layer for polymer tandem solar cells. Nano Lett 2014;14(3):1467.
[16] Iruretagoyena D, Huang X, Shaffer MSP, Chadwick D. Influence of alkali metals (Na, K, and Cs) on CO2 adsorption by layered double oxides supported on graphene oxide. Ind Eng Chem Res 2015;54(46):11610–8.
[17] Berry V. Impermeability of graphene and its applications. Carbon 2013;62:1.
[18] Naghdi S, Nešović K, Mišković-Stanković V, Rhee KY. Comprehensive electrochemical study on corrosion performance of graphene coatings deposited by chemical vapour deposition at atmospheric pressure on platinum-coated molybdenum foil. Corros Sci 2018;130:31.
[19] Naghdi S, Jevremović I, Mišković-Stanković V, Rhee KY. Chemical vapour deposition at atmospheric pressure of graphene on molybdenum foil: effect of annealing time on characteristics and corrosion stability of graphene coatings. Corros Sci 2016;113:116.
[20] Naghdi S, Rhee KY, Park SJ. Oxidation resistance of graphene-coated molybdenum: effects of pre-washing and hydrogen flow rate. Int J Refract Metals Hard Mater 2017;65:29.
[21] Mišković-Stanković V, Jevremović I, Jung I, Rhee K. Electrochemical study of corrosion behavior of graphene coatings on copper and aluminum in a chloride solution. Carbon 2014;75:335.
[22] Singh Raman RK, Chakraborty Banerjee P, Lobo DE, Gullapalli H, Sumandasa M, Kumar A, et al. Protecting copper from electrochemical degradation by graphene coating. Carbon 2012;50:4040.
[23] Yu F, Camilli L, Wang T, Mackenzie DMA, Curioni M, Akid R, et al. Complete long-term corrosion protection with chemical vapor deposited graphene. Carbon 2018;132:78.
[24] Ren S, Cui M, Li W, Pu J, Xue Q, Wang L. N-doping of graphene: toward long-term corrosion protection of Cu. J Mater Chem A 2018;6:24136.
[25] Kumar AM, Babu RS, Obot I, Gasem ZM. Fabrication of nitrogen doped graphene oxide coatings: experimental and theoretical approach for surface protection. RSC Adv 2015;5:19264.
[26] Briere T, Sommer A. Low-work-function surfaces produced by cesium carbonate decomposition. J Appl Phys 1977;48:3547.
[27] Merel P, Tabbal M, Chaker M, Moisa S, Margot J. Direct evaluation of the sp^3 content in diamond-like-carbon films by XPS. Appl Surf Sci 1998;136:105.
[28] Al-Kuhaili M. Characterization of copper oxide thin films deposited by the thermal evaporation of cuprous oxide (Cu_2O). Vacuum 2008;82:623.
[29] Krishnan N, Delgass W, Robertson W. Electron binding energies of core levels in caesium adsorbed on a nickel (100) surface. J Phys F Met Phys 1977;7:2623.
[30] Yang HB, Dong YQ, Wang X, Khoo SY, Liu B. Cesium carbonate functionalized graphene quantum dots as stable electron-selective layer for improvement of inverted polymer solar cells. ACS Appl Mater Interfaces 2014;6:1092.
[31] Giovannetti G, Khomyakov P, Brocks G, Karpan Vv, Van den Brink J, Kelly PJ. Doping graphene with metal contacts. Phys Rev Lett 2008;101:026803.
[32] Ferrari AC, Basko DM. Raman spectroscopy as a versatile tool for studying the properties of graphene. Nat Nanotechnol 2013;8:235.
[33] Ni Z, Wang Y, Yu T, Shen Z. Raman spectroscopy and imaging of graphene. Nano Res 2008;1:273.
[34] Mafra D, Samsonidze G, Malard L, Elias DC, Brant JC, Plentz F, et al. Determination of LA and TO phonon dispersion relations of graphene near the Dirac point by double resonance Raman scattering. Phys Rev B 2007;76:233407.
[35] Tuinstra F, Koenig JL. Raman spectrum of graphite. J Chem Phys 1970;53:1126.
[36] De M, Hajra S, Tiwaria R, Sahoo S, Choudhary RNP, Tewari HS. Structural, dielectric and electrical characteristics of BiFeO3-NaNbO3 solid solutions. Ceram Int 2018;44(10):11792.
[37] Hajra S, Sahoo S, Das R, Choudhary RNP. Structural, dielectric and impedance characteristics of (Bi0.5Na0.5)TiO3-BaTiO3 electronic system. J Alloys Compd 2018;750:507.
[38] Hajra S, Tripathy A, Panigrahi BK, Choudhary RNP. Development and excitation performance of lead free electronic material: Eu and Fe doped Bi0.5Na0.5TiO3 for filter application. Mater Res Express 2019;6(7):1.
[39] Jauregui LA, Cao H, Wu W, Yu Q, Chen YP. Electronic properties of grains and grain boundaries in graphene grown by chemical vapor deposition. Solid State Commun 2011;151(16):1100–4.
[40] Sim U, Yang T-Y, Moon J, An J, Hwang J, Seo J-H, et al. N-doped monolayer graphene catalyst on silicon photocathode for hydrogen production. Energy Environ Sci 2013;6:3658.
[41] Lu X, Xie X, Luo J, Sun J. Cesium-doped graphene grown in situ with ultra-small TiO_2 nanoparticles for high-performance lithium-ion batteries. New J Chem 2017;41:7938.
[42] Naghdi S, Sanchez-Arriaga G. Work function tuning of graphene oxide by using cesium applied to low work function tethers. arXiv preprint 2019, arXiv:1907.03656.
[43] Luo Z, Yu T, Ni Z, Lim S, Hu H, Shang J, et al. Electronic structures and structural evolution of hydrogenated graphene probed by Raman spectroscopy. J Phys Chem C 2011;115:1422.

[44] Zhou F, Li Z, Shenoy GJ, Li L, Liu H. Enhanced room-temperature corrosion of copper in the presence of graphene. ACS Nano 2013;7:6939.
[45] Shin HJ, Choi WM, Choi D, Han GH, Yoon S-M, Park H-K, et al. Control of electronic structure of graphene by various dopants and their effects on a nanogenerator. J Am Chem Soc 2010;132:15603.
[46] Li DY. Electron work function at grain boundary and the corrosion behavior of nanocrystalline metallic materials. Mater Res Soc Symp Proc 2006;887:227.
[47] Li W, Li DY. Influence of surface morphology on corrosion and electronic behavior. Acta Mater 2006;54:445.
[48] Li W, Li DY. Variations of work function and corrosion behaviors of deformed copper surfaces. Appl Surf Sci 2005;240:388.
[49] Kear G, Barker BD, Walsh FC. Electrochemical corrosion of unalloyed copper in chloride media—a critical review. Corros Sci 2004;46:109.
[50] Trachli B, Keddam M, Takenouti H, Srhiri A. Protective effect of electropolymerized 3-amino 1,2,4-triazole towards corrosion of copper in 0.5 M NaCl. Corros Sci 2002;44:997.
[51] Curkovic HO, Stupnisek-Lisac E, Takenouti H. The influence of pH value on the efficiency of imidazole based corrosion inhibitors of copper. Corros Sci 2010;52:398.
[52] Hsu C, Mansfeld F. Technical note: concerning the conversion of the constant phase element parameter Y0 into a capacitance. Corrosion 2001;57:747.
[53] Petrović M, Rakić IŠ, Runte S, Busse C, Sadowski JT, Lazić P, et al. The mechanism of caesium intercalation of graphene. Nat Commun 2013;4:2772.
[54] Qiu Y, Zhang X, Yang S. High performance supercapacitors based on highly conductive nitrogen-doped graphene sheets. Phys Chem Chem Phys 2011;13:12554.